I&EC research
Industrial & Engineering Chemistry Research

Article

pubs.acs.org/IECR

Fabrication of (Calcein−ZnS)$_n$ Ordered Ultrathin Films on the Basis of Layered Double Hydroxide and Its Ethanol Sensing Behavior

Ying Guo, Yaping Xiao, Limin Zhang, and Yu-Fei Song*

State Key Laboratory of Chemical Resource Engineering, Beijing University of Chemical Technology, P.O. Box 98, Beijing, 100029, P.R. China

Supporting Information

ABSTRACT: (Calcein−ZnS)$_n$ ultrathin films (UTFs) were fabricated through a two-step procedure including the layer-by-layer (LBL) assembly of calcein and exfoliated Zn_2Al layered double hydroxide (LDH) nanosheets, followed by an in situ gas/solid reaction with H_2S. The assembly process of calcein and exfoliated LDH was monitored by UV−vis absorption measurements to get a stepwise and regular growth of the (calcein−LDH)$_n$ UTFs upon increasing the deposited cycles. By an in situ gas−solid reaction with H_2S, the resulting sulfurization derivatives denoted as (calcein−ZnS)$_n$ UTFs were obtained. The resulting (calcein−ZnS)$_{30}$ UTF possesses high ethanol sensing performance (response value is 8.9−100 ppm ethanol) at relatively low working temperature (90 °C). The LBL assembly process and chemical conversion technique based on Zn_2Al−LDH combine the functional organic molecules and inorganic semiconductor, which enables us to develop innovative composite materials with adjustable compositions for a broad range of applications.

1. INTRODUCTION

Gas sensors are greatly applied in the biomedical, chemical, and food industries.[1] For example, ethanol sensors are widely used to detect alcohol on human breath, to detect leaks in industrial distribution lines, to evaluate the wine quality, as well as to monitor the food and biomedical safety, etc.[2,3] Because of the great demands of gas sensors with high sensitivity, good selectivity, and long-term stability, so-called "3S" great efforts have been made to fabricate novel sensing materials since the first chemresisitive metal oxide-based gas sensor was prepared. Until now, apart from conventional semiconductor oxide, gas sensing materials have extended to conductive polymer, organic compounds, carbon nanotubes, etc.[4] Furthermore, the size and shape of gas sensing materials are also adjustable from the micrometer to nanometer scale in the form of particles, rods, wires, belts, quantum dots, fibers, and even core−shell structures, which are critical to their gas sensing capabilities.[5,6] Nevertheless, the fabrication and manufacture techniques, which are as important as new materials themselves, remain to be explored and developed. It should be noted that a large number of sensing materials have been prepared and deposited for gas sensing applications as thin film, which involves, namely, the physical (dry) and chemical (wet) techniques. The physical techniques include chemical vapor deposition, thermal vapor deposition, sputtering, laser ablation, etc., whereas the chemical techniques include sol−gel, Langmuir−Blodgett, spin coating, LBL assembly, etc.[7] The advantage of gas sensing films via the chemical route is that a large quantity of processable nanostructures can be obtained in a cost-effective, highly scalable, and mild reaction condition. In particular, organic−inorganic hybrid thin films cannot be prepared by the standard physical techniques because the vapor pressure and decomposition temperature of the organic and inorganic individual compounds differ significantly.[8] As such, among the methods that have been developed for preparing thin films, LBL assembly, based on sequential adsorptions of oppositely charged species in aqueous solution, is a unique method for the deposition of composite films with controllable thickness at a molecular scale and the merits of low cost, room temperature process, and high reproducibility.[9−14] It is worth noting that to the best of our knowledge there are few reports regarding the preparation of gas sensing composite thin films with the combination of organic molecule and inorganic semiconductor through the LBL assembly approach.

Organic molecule calcein (Scheme S1 of the Supporting Information) and its derivatives are mainly used for detecting metal ions (Ca^{2+}, Cu^{2+}, Fe^{2+}, Zn^{2+}, Mn^{2+}, and Fe^{3+}) and for DNA fluorescent sensor.[15−17] Previous reports have also shown that the composites films of calcein−PAN [calcein-poly(acrylonitrile)], calcein−HMDA (hexamethylene diamine), calcein-poly(ethylene oxide)/poly(acrylic acid), or thermally deposited calcein films could be applied for ammonia sensor or humidity sensor.[18−20]

Layered double hydroxides (LDHs) are a family of anionic lamellar hydrotalcite-like clays with the general formula of $[M^{2+}_{1-x}M^{3+}_{x}(OH)_2][A^{n-}_{x/n}\cdot mH_2O]$, in which M^{2+} and M^{3+} are divalent and trivalent metal cations respectively, and A^{n-} is the intercalated guest anion. LDHs have been widely employed as catalysts, adsorbents, anion exchangers, precursors, magnetics, and electrodes for alkaline secondary batteries, etc.[21−24] Previous experiments have shown that Cd- or Zn-containing LDH can be used as a template to generate CdS or ZnS nanoparticles implanted in the matrix of host layers.[25,26] As such, it is promising to build ZnS assembly films from a template of Zn_2Al−LDH. Additionally, as a wide band gap

Received: April 12, 2012
Revised: June 13, 2012
Accepted: June 15, 2012
Published: June 15, 2012

semiconductor of ZnS, ZnS-based materials have also been investigated for sensors, such as for UV-light sensors,[27] biosensors,[28] and humidity sensors,[29] as well as for gas sensors,[30−32] etc. Furthermore, it has also been reported that LDHs can be delaminated into nanosheets, which allow us to obtain positively charged single nanosheets.[33−36] One of the most important and attractive applications of such exfoliated nanosheets is that they could serve as two-dimensional building blocks to construct UTFs with superior functionalities.[37−39]

Herein, in this paper, $(calcein−LDH)_n$ UTFs have been prepared by LBL assembly of calcein with exfoliated layered double hydroxides $Zn_2Al−LDH$ (Scheme 1), which is followed by an in situ gas−solid sulfurization of $(calcein−LDH)_n$ UTFs. The exfoliated nanosheets of $Zn_2Al−LDH$ have been utilized as templates for the preparation of ZnS implanted in the inorganic building blocks. Generally, the two-step process including the LBL assembly of calcein with exfoliated LDH and the in situ gas−solid sulfurization process provides an approach for preparing organic molecule−inorganic semiconductor composite UTFs, which might have superior gas sensing properties to one compound alone.

Scheme 1. LBL Assembly Process for $(Calcein−LDH)_n$ UTF and $(Calcein−ZnS)_n$ UTF

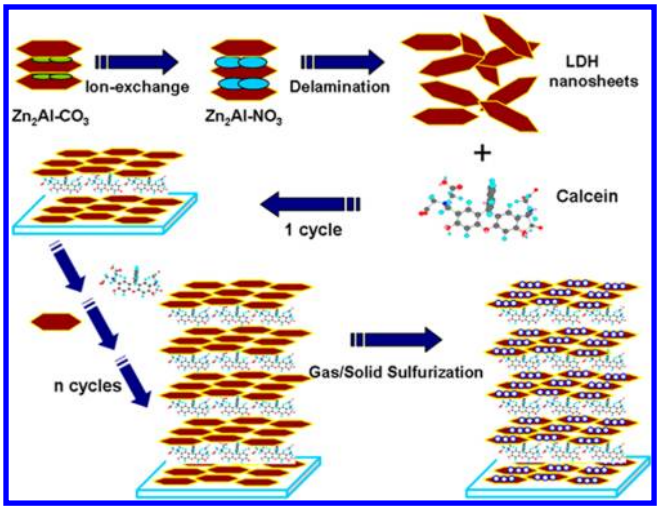

2. EXPERIMENTAL SECTION

2.1. Synthesis of $Zn_2Al−LDH$ and Nitrate−Intercalated LDH. $Zn_2Al−LDH$ was synthesized using a hydrolysis method under hydrothermal conditions on the basis of a previous report with slight modification by replacing cobalt salt with zinc salt.[37] A typical preparation process is described as follows: $Zn(NO_3)_2·6H_2O$ (0.002 mol), $Al(NO_3)_3·9H_2O$ (0.001 mol), and urea (0.012 mol) were dissolved in aqueous solution. The mixture was sealed in a Teflon-lined stainless steel autoclave and heated at 100 °C for 24 h. The obtained CO_3^{2-} LDH ($Zn_2Al−CO_3$) was washed with water and dried in air at 60 °C. Afterward, this sample was converted to NO_3^- form by ion exchange using a $NaNO_3$ and HNO_3 solution while purging with nitrogen gas for 1 day at ambient temperature. The precipitate ($Zn_2Al−NO_3$) was separated through centrifugation, washed with distilled water, and dried under vacuum.

2.2. Fabrication of $(Calcein/LDH)_n$ UTFs. The delamination of $Zn_2Al−NO_3$ was conducted according to that described by Sasaki et al.[21] A total of 0.1 g of $Zn_2Al−NO_3$ was shaken in a 100 mL formamide solution for 24 h to produce a colloidal suspension of exfoliated $Zn_2Al−NO_3$ nanosheets. A clear Tyndall light scattering was observed, and the well-dispersed colloidal suspension was transparent and stable. The quartz glass substrate was first cleaned in concentrated NH_3/30% H_2O_2 (7:3) and concentrated H_2SO_4 for 30 min each. After each procedure, the quartz substrate was rinsed and washed thoroughly with deionized water. The substrate was dipped in the colloidal suspension of LDH nanosheets for 10 min followed by washing thoroughly with deionized water, and then the substrate was treated with a 100 mL of calcein aqueous solution (0.025 wt %, pH was adjusted to 7.0 by NaOH) for 10 min. The washing procedure of calcein was the same as that for the LDH nanosheets described above. $(Calcein/LDH)_n$ UTFs were fabricated by depositing alternatively with a LDH nanosheets suspension and calcein solution for n cycles. The resulting films were dried under a nitrogen gas flow for 2 min at ambient temperature.

2.3. Sample Characterization. Powder X-ray diffraction (XRD) analysis was conducted on a Shimadzu XRD-6000 powder diffractometer using Cu Ka radiation at an accelerating voltage of 40 kV and current of 30 mA. The Fourier transform infrared (FTIR) spectra were recorded in the range of 400−4000 cm^{-1} on a Nexus 670 spectrometer. The solid UV−vis absorption spectra were collected in the range from 190 to 800 nm on a Shimadzu U-3000 spectrophotometer. The morphol-

Scheme 2. Gas Sensing Analysis System

dx.doi.org/10.1021/ie300966t | Ind. Eng. Chem. Res. 2012, 51, 8966−8973

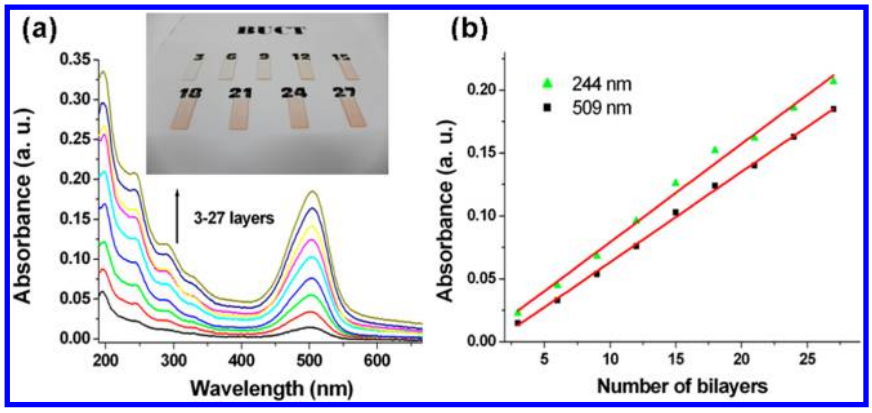

Figure 1. (a) UV−vis absorption spectra of the $(calcein−LDH)_n$ (n = 3−27) UTFs. (b) Linear relationship between absorbance at 244 and 509 nm and bilayer number n. Inset: Photographs of $(calcein−LDH)_n$ (n = 3−27) UTFs in (a).

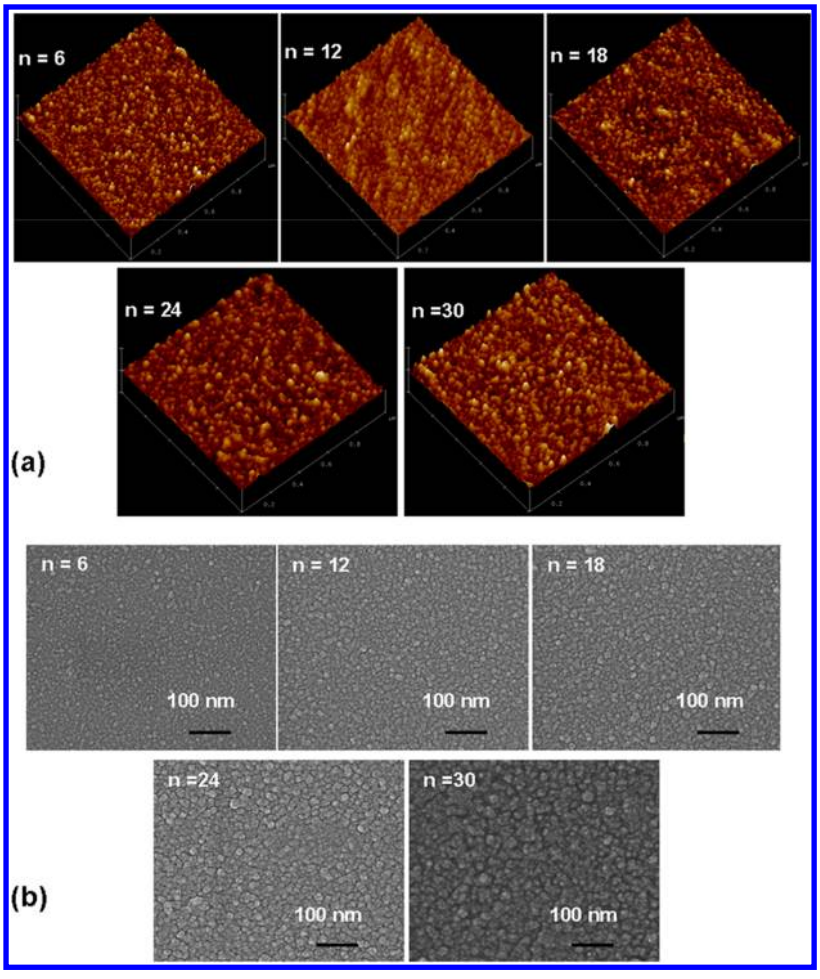

Figure 2. (a) AFM images and (b) top-view of SEM of $(calcein−LDH)_n$ UTFs with n = 6, 12, 18, 24, and 30, respectively.

ogy and thickness data of thin films were investigated by using a scanning electron microscope (SEM Hitachi S-4700), and the accelerating voltage applied was 20 kV. The surface roughness of the UTFs was examined using an Agilent AFM-5500 atomic force microscopy.

2.4. Gas Sensing Measurements. In this paper, $(calcein−LDH)_{30}$ UTF and $(calcein−ZnS)_{30}$ UTF have been used for gas sensing measurement. The gas sensing properties of the UTFs were measured by a CGS-1TP intelligent gas sensing analysis system (Beijing Elite Tech. Co. Ltd., China). This multifunctional system consists of a heating system, gas distribution system, probe adjustment system, vacuum system, measurement and data acquisition system, and measurement control software (Scheme 2). The heating system offers an external temperature control (from room temperature to about 500 °C with a precision of 1 °C), which could adjust the sensor temperature directly. All the materials were preheated at different working temperature for about 30 min. When the resistances of the sensors were stable, target gas was injected into the test chamber (18 L in volume) by the dynamic gas distributing system. After the sensor resistances reached new constant values, the test chamber was opened to recover the

dx.doi.org/10.1021/ie300966t | Ind. Eng. Chem. Res. 2012, 51, 8966−8973

sensors in air. The whole experimental process was performed in a superclean room at a constant humidity (25% relative humidity) and temperature (20 °C). The working temperature of the sensors was reported by the analysis system automatically.

The response was designated as *Ra*/*Rg*, where *Ra* was the sensor resistance in air (base resistance), and *Rg* was that in target gas. The time taken by the sensor resistance to change from *Ra* to *Ra* − 90% × (*Ra* − *Rg*) was defined as response time when the target gas was introduced to the sensor, and the time taken from *Rg* to *Rg* + 90% × (*Ra* − *Rg*) was defined as recovery time when the ambience was replaced by air.

3. RESULTS AND DISCUSSION

3.1. Powder X-ray Diffraction (XRD) Analysis of LDH Precursor. The XRD pattern of the $Zn_2Al{-}CO_3$ is shown in Figure S1 of the Supporting Information. The obtained composite is typical for LDHs in the carbonate form. As the NO_3^- LDH intercalated LDH is found to possess excellent delamination behavior, $Zn_2Al{-}NO_3$ was synthesized via a conventional anion exchange of $Zn_2Al{-}CO_3$ with an aqueous solution of $NaNO_3$ and HNO_3. As shown in Figure S1 of the Supporting Information, the gallery height increases from 0.75 nm of $Zn_2Al{-}CO_3$ to 0.89 nm of $Zn_2Al{-}NO_3$, suggesting the successful exchange of the guest anion from CO_3^{2-} to NO_3^- in the LDH.[37] The absorption band of CO_3^{2-} at 1354 cm^{-1} in the FT-IR spectra (Figure S2 of the Supporting Information) of $Zn_2Al{-}CO_3$ disappears after the ion exchange process and a new absorption band appears at 1385 cm^{-1}, which provide further proof for the successful exchange from CO_3^{2-} to NO_3^-.

3.2. UV−Vis Absorption Spectroscopy of (Calcein/LDH)$_n$ UTFs. Multilayer films were obtained by alternately dipping a quartz glass slide or silicon wafer into a colloidal suspension of the LDH nanosheets and calcein solution. The multilayer build-up process of the film was monitored by UV−vis spectroscopy after each deposition cycle (shown in Figure 1(a)). From the UV spectra of the (calcein−LDH)$_n$ UTFs, the strong absorption band is at 509 nm, which is consistent with the light-yellow color of the UTFs.[17] The absorption band at 190, 244, and 290 nm could be assigned to the $\pi-\pi^*$ transition of C═O bonds, conjugated $\pi-\pi^*$ transition of the aromatic C−C bonds, and $n-\pi^*$ transitions of C═O bonds, respectively. Figure 1(b) shows the dependence of absorption at 244, 290, and 509 nm against the number of deposition units. It is shown that the absorption increases linearly with an increase in deposition cycles, which indicates a stepwise and regular film growth in thickness. This is also confirmed by the gradual increase in the color intensity of the UTFs with the increasing number of bilayers.

3.3. Morphology and Structural Characterization of (Calcein/LDH)$_n$ UTFs. The deposited process of (calcein−LDH)$_n$ UTFs was further monitored by atomic force microscopy and scanning electron microscopy (AFM and SEM). The AFM topographical images give the root-mean-square (rms) surface roughness of the UTFs (n = 6−30) (Figure 2(a)). The value of root-mean-square (rms) roughness for the UTFs increases slowly with the number of deposition cycles (Table 1) from 1.9 nm for 6 bilayers (n = 6) to 4.9 nm for 30 bilayers (n = 30), indicating that all the films have relatively smooth surfaces

A typical top view of the SEM images (Figure 2(b)) for (calcein−LDH)$_n$ UTFs also confirm that the films surfaces are microscopically smooth and uniform. Moreover, the continuous and homogeneous UTFs can be further observed from the side view of the SEM images (Figure 3) with the thicknesses of the as-prepared UTFs (n = 6−30) in the range of 10−56 nm. The approximately linear increase in the thickness with n confirms that the UTFs possess a uniform and periodic layered structure. It thus can be estimated that the average thickness of one bilayer (calcein−LDH)$_{n=1}$ is about 1.8 nm.

Table 1. Depth and Thickness Parameters for the (Calcein/LDH)$_n$ UTFs with 6, 12, 18, 24, 30 Bilayers

n	6	12	18	24	30
rms roughness (nm)[a]	1.9	2.6	3.3	4.1	4.9
SEM thickness (nm)[b]	ca. 10	ca. 20	ca. 34	ca. 48	ca. 56

[a]Values of statistical rms roughness were obtained by AFM. [b]SEM thicknesses were obtained from the side view of (calcein−LDH)$_n$ UTFs.

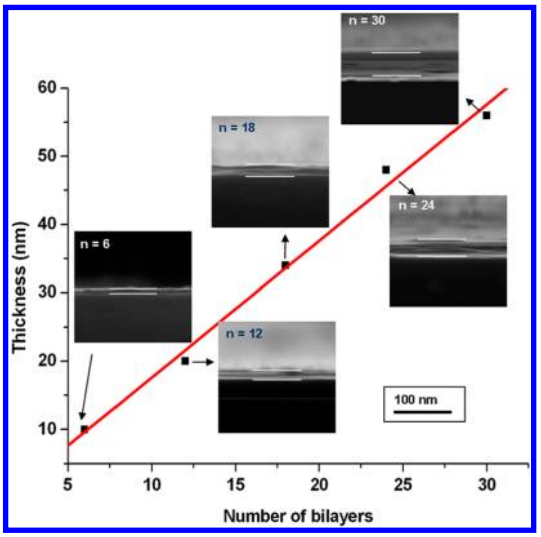

Figure 3. Plot of the thickness of the (calcein−LDH)$_n$ UTFs as a function of n. Insets show the side view of the SEM with n = 6, 12, 18, 24, and 30, respectively.

3.4. In Situ Sulfurization of (Calcein/LDH)$_n$ UTFs. The (calcein−LDH)$_n$ UTFs with different n values were sealed in a glass vessels, which were evacuated before excessive H_2S gas was injected into the vessel. Upon introduction of the H_2S gas, the color of the UTFs in the vessel turned from light red to light yellow. The reaction was held for 2 h at room temperature in order to ensure that the precursors were sulfurized completely. All the UTFs were subjected to the gas−solid sulfurization reaction separately to form ZnS implanted in the inorganic layers of the UTFs.

It is shown that the transparent light-red color of (calcein−LDH)$_n$ UTFs changed to light yellow after sulfurization. The UV−vis spectra of the (calcein−ZnS)$_n$ UTFs are shown in Figure 4 (a). The absorption peaks of the films in the whole spectral region decrease, and the main absorption peaks of the films blue shift gradually from 244 to 237 nm and from 509 to 481 nm, respectively. Furthermore the absorption at 290 nm becomes inconspicuous. Compared with the absorption of (calcein−LDH)$_n$ UTFs, the observed blue shift may be attributed to the formation of ZnS and interactions between ZnS and calcein. ZnS is n-type semiconductor that has excess electrons, and its UV−vis absorption usually appears below 400 nm.[40] The presence of ZnS might destroy the conjugated

dx.doi.org/10.1021/ie300966t | Ind. Eng. Chem. Res. 2012, 51, 8966−8973

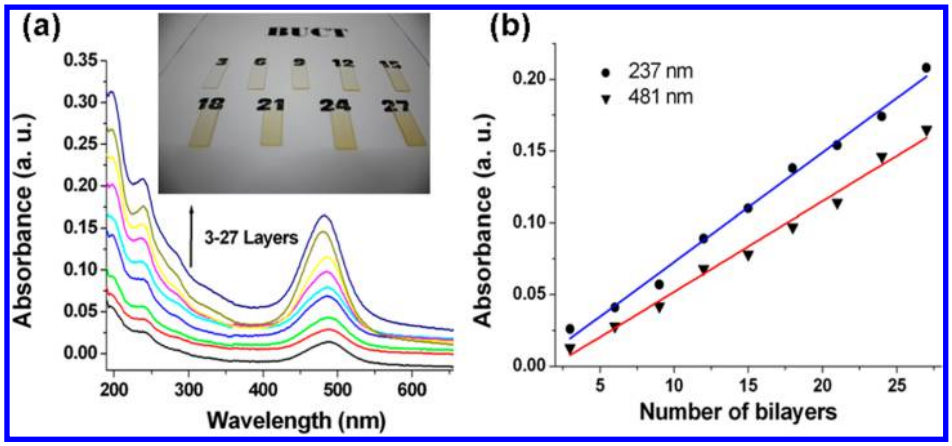

Figure 4. (a) UV−vis absorption spectra of the $(calcein−ZnS)_n$ (n = 3−27) UTFs. (b) Linear relationship between absorbance at 237 and 481 nm and bilayer number n. Inset: Photographs of $(calcein−ZnS)_n$ (n = 3−27) with different bilayer numbers (n) in (a).

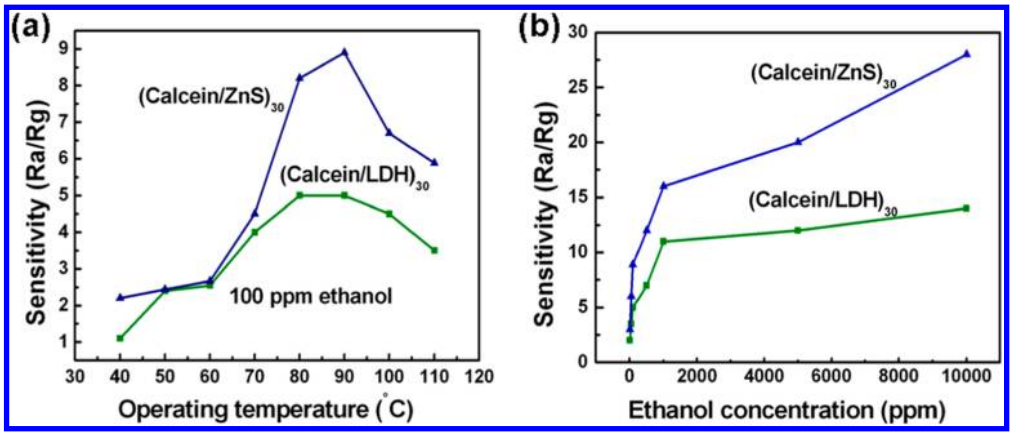

Figure 5. (a) Response vs working temperature of $(calcein−LDH)_{30}$ UTF and $(calcein−ZnS)_{30}$ UTF exposed to 100 ppm ethanol. (b) Response of $(calcein−LDH)_{30}$ UTF and $(calcein−ZnS)_{30}$ UTF to different concentration of ethanol.

system of calcein and weaken the planar electron transition of calcein, which induced a decrease in the absorption intensity and the blue shift of the absorption peak, and the color of the UTFs changes from light red to light yellow, which is in accordance with the absorption changing from 509 to 481 nm. Figure 4(b) shows the dependence of absorption at 237 and 481 nm against the number of deposition units. It is shown that the absorption still increases linearly with an increase in the deposition cycles even after sulfurization process, which indicates the sulfurization process does not destroy the regularity of the UTFs.

3.5. Ethanol Gas Sensing Characterization for $(Calcein−LDH)_n$ UTFs, and $(Calcein−ZnS)_n$ UTFs(n = 30). In this paper, we observed the ethanol-sensing behavior through measuring the change of the resistance of UTFs. The principle of the gas detection of resistance-type sensors is based on the conductance variation of the sensing element, which depends on the gas atmosphere and the working temperature of the sensing materials exposed to the test gas.[41] The responses of the $(calcein−LDH)_{30}$ UTF and $(calcein−ZnS)_{30}$ UTF to 100 ppm ethanol at various temperatures are shown in Figure 5 (a).

Both UTFs exhibit different sensing properties in all the tests. As shown, the responses are improved by increasing the working temperature below 80 °C for $(calcein−LDH)_{30}$ and below 90 °C for $(calcein−ZnS)_{30}$, which can be explained by the enhanced activation of the materials. In ethanol gas-sensing, oxygen sorption plays an important role in electrical transport properties of $(calcein−LDH)_{30}$ UTF and $(calcein−ZnS)_{30}$ UTF. It should be noted that chemisorbed oxygen species depend strongly on temperature. At low temperatures, O_2^- is commonly chemisorbed, whereas at high temperatures, O_2^{2-} and O^- are commonly chemisorbed, while O_2^- disappears rapidly. Hence, the resistance of UTF decreases with the elevating temperature, which is shown in Figure 5 (a). When the working temperature continues increasing, the desorption process of adsorbed oxygen becomes dominant, and the concentration of chemisorbed oxygen decreases, which results in the declined response. Therefore, the maximal response is obtained on the basis of $(calcein−LDH)_{30}$ at a working temperature of 80 °C and $(calcein−ZnS)_{30}$ at a working temperature of 90 °C, respectively, and because the highest response of $(calcein−ZnS)_{30}$ is at the temperature of 90 °C, all the tests below are focused on this sample at 90 °C.

At constant temperature, the response changes with gas concentrations. Figure 5(b) depicts the correlation between the concentration and responses of $(calcein−LDH)_{30}$ UTF and $(calcein−ZnS)_{30}$ UTF at the working temperature of 90 °C. Both UTFs can detect ethanol gas down to 10 ppm, and the corresponding values are 3 for $(calcein−ZnS)_{30}$ and 2 for $(calcein−LDH)_{30}$, respectively. With an increase in gas concentration, the responses increase remarkably. The responses are 3.5, 5, 7, 11, 12, and 14 for $(calcein−LDH)_{30}$ to 50, 100, 500, 1000, 5000, and 10000 ppm ethanol, and the

dx.doi.org/10.1021/ie300966t | Ind. Eng. Chem. Res. 2012, 51, 8966−8973

corresponding values for $(calcein–ZnS)_{30}$ are 6, 8.9, 12, 16, 20, and 28, respectively. This can be explained as the more ethanol concentration increases, the more electrons from the chemisorbed oxygen species are released, which further leads to an increased conductivity of the UTFs.

From Figure 5, it is found $(calcein–ZnS)_{30}$ UTF always shows higher response than $(calcein–LDH)_{30}$ UTF when they were put at the same working temperature and exposed to equal concentrations of ethanol. This result also reveals that the presence of ZnS brought the high response of $(calcein–ZnS)_{30}$ UTF to ethanol gas, and this phenomenon can be clarified by the mechanisms of ethanol sensing, which is described as follows: When the UTFs are surrounded by air, oxygen molecules are adsorbed on the surface to form chemisorbed oxygen species (O_2^-, O_2^{2-}, and O^-) by capturing electrons from the conduction band of UTFs. In $(calcein–LDH)_{30}$ UTF, the active sites to adsorb oxygen molecules are mainly calcein molecules. However, compared with $(calcein–LDH)_{30}$ UTF, there are another two simultaneous steps in $(calcein–ZnS)_{30}$ UTF to complete the adsorbed process of the oxygen molecule when exposed to air ambient (Figure 6). These steps are that

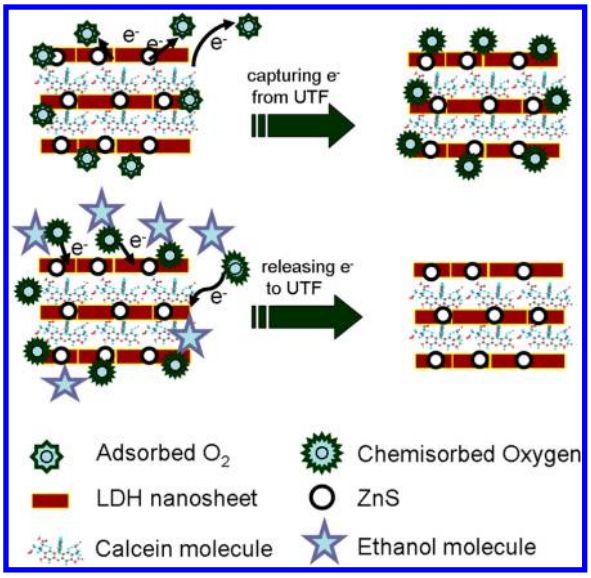

Figure 6. Schematic representation of gas-sensing mechanism for $(calcein–ZnS)_{30}$ UTF.

the presence of ZnS in $(calcein–ZnS)_{30}$ UTF provides more active sites, which can adsorb more oxygen species than $(calcein–LDH)_{30}$ UTF. Differing from most semiconductor sensors, the ZnS-based sensor has another parallel path to adsorb oxygen molecules. ZnS has fertile trapped surface states, sulfur vacancy, and interstitial sulfur lattice defects.[32,42] These states can further accelerate the adsorbing of oxygen molecules from the surroundings and the depletion of free electron from the conduction band in the $(calcein–ZnS)_{30}$ UTF, resulting in decreased conductivity of the UTF. Once the target ethanol gas is introduced, the reductive ethanol gas reacts with the ionic oxygen species, and then the electrons trapped by the chemisorbed oxygen species are released to the UTF, leading to increased conductivity of the UTF and thus an elevated response of ethanol sensing. Consequently, the specific surface states of the $(calcein–ZnS)_{30}$ UTF play an important role in the contact and subsequent reaction of oxygen species with the ethanol gas, which clarifies very well about why $(calcein–ZnS)_{30}$ UTF always has a better response than $(calcein–LDH)_{30}$ UTF in our studies. Furthermore, the coexistense of ZnS and calcein might have some interactions between them, which play a synergistic effect on ethanol sensing and result in a high response of $(calcein–ZnS)_{30}$ UTF to ethanol gas. Further investigations are proceeding in our lab.

Response and recovery speeds are vital parameters to evaluate the performance of sensing materials, especially when for most low working temperature sensing materials, their response and recovery time are comparatively long due to their low activation at low temperature. However, the current $(calcein–ZnS)_{30}$ UTF exhibits very quick response behavior to ethanol gas at 90 °C. When the reductive ethanol gas is introduced, the electron releasing process begins. The ethanol gas reacts with the surface oxygen species, which causes an increase in the conductivity of the $(calcein–ZnS)_{30}$ UTF and thus an increase in the *Ra*/*Rg* value of the UTF. Whereas, when the UTF is exposed to air again, the electron capturing process starts, which decreases the conductivity of the $(calcein–ZnS)_{30}$ UTF and thus decreases the *Ra*/*Rg* value of the UTF. As shown in Figure 7, the response and recovery time are calculated to be

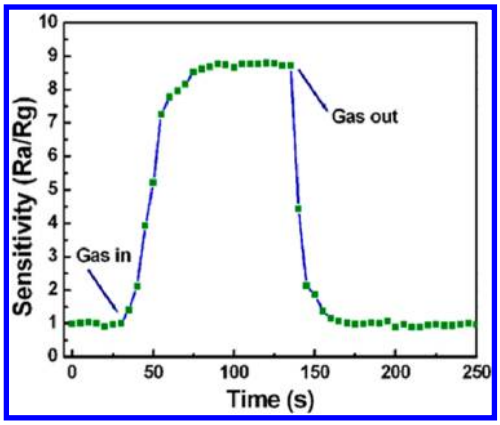

Figure 7. Response of $(calcein–ZnS)_{30}$ UTF to 100 ppm of ethanol at working temperature of 90 °C.

45 and 15 s, respectively. The advantage of $(calcein–ZnS)_{30}$ UTF in a fast response performance might be attributed to the microstructure of this UTF.

Furthermore, the selectivity of chemical sensor is also an important factor for further application. It is found that the $(calcein–ZnS)_{30}$ UTF exhibits higher response to ethanol but less response to toluene, NH_3, and very low response to 100 ppm of H_2, CO, C_2H_2, and CH_4 at 90 °C, indicating that the $(calcein–ZnS)_{30}$ UTF is a good candidate for highly selective detection of ethanol.

4. CONCLUSIONS

This work reported an approach for fabricating ordered assembly film of organic molecule calcein with semiconductor ZnS. Zn_2Al–LDH here serves both as a self-assembly unit and a template for the preparation of ZnS. The $(calcein–ZnS)_{30}$ UTF shows high and fast response as well as short recovery time to ethanol gas at 90 °C. Meanwhile, the presence of ZnS in the $(calcein–ZnS)_{30}$ UTF largely improves the response to ethanol. Future investigation of ZnS-based or calcein-based sensors for ethanol or other important volatile organic compounds as well as the possible effect of M^{3+} in the LDH nanosheets to gas sensing are in progress in our lab.

dx.doi.org/10.1021/ie300966t | *Ind. Eng. Chem. Res.* 2012, 51, 8966–8973

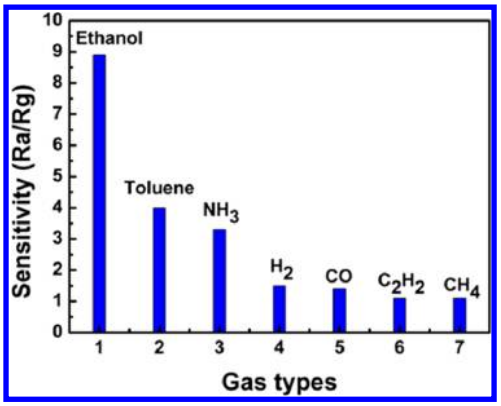

Figure 8. Gas responses of $(calcein–ZnS)_{30}$ UTF to 100 ppm of different gases at working temperature of 90 °C.

■ ASSOCIATED CONTENT

Supporting Information

Molecular structure of calcein, FT-IR spectra, and XRD patterns of $Zn_2Al–CO_3$ and $Zn_2Al–NO_3$. This information is available free of charge via the Internet at http://pubs.acs.org/.

■ AUTHOR INFORMATION

Corresponding Author

*Tel: (+86)-10-64431832. E-mail: songyufei@hotmail.com or songyf@mail.buct.edu.cn.

Notes

The authors declare no competing financial interest.

■ ACKNOWLEDGMENTS

This work was supported by the National Natural Science Foundation of China (21001014, 21076020), Beijing Natural Science Foundation (2113049), Fundamental Research Funds for the Central Universities (QN0908, ZZ1227), the program for New Century Excellent Talents of the Ministry of Education of China (NCET-09-0201), and the Beijing Nova Program (2009B12). We thank Dr. Qi Qi and Beijing Elite Tech Co. Ltd., China, for gas sensing measurements.

■ REFERENCES

(1) Adachi, G.; Imanaka, N. Chemical Sensors. *Handbook on the Physics and Chemistry of Rare Earths*; Elsevier: The Netherlands, 1995; Chapter 123, p 21.

(2) Kauffman, D. R.; Star, A. Carbon nanotube gas and vapor sensors. *Angew. Chem., Int. Ed.* **2008**, *47*, 6550–6570.

(3) Zhang, Z.; Zhang, C.; Zhang, X. Development of a chemiluminescence ethanol sensor based on nanosized ZrO_2. *Analyst* **2002**, *127*, 792–796.

(4) Jiménez-Cadena, G.; Riu, J.; Rius, F. X. Gas sensors based on nanostructured materials. *The Analyst* **2007**, *132*, 1083–1099.

(5) Tricoli, A.; Righettoni, M.; Teleki, A. Semiconductor gas sensors: Dry synthesis and application. *Angew. Chem., Int. Ed.* **2010**, *49*, 632–7659.

(6) Huang, X. J.; Choi, Y. K. Chemical sensors based on nanostructured materials. *Sens. Actuators, B* **2007**, *122*, 659–671.

(7) Ho, G. W. Gas sensor with nanostructured oxide semiconductor materials. *Sci. Adv. Mater.* **2011**, *3*, 150–168.

(8) Du, N.; Zhang, H.; Chen, B. D.; Ma, X. Y.; Liu, Z. H.; Wu, J. B.; Yang, D. R. Porous indium oxide nanotubes: Layer-by-layer assembly on carbon-nanotube templates and application for room-temperature NH_3 gas sensors. *Adv. Mater.* **2007**, *19*, 1641–1645.

(9) Kim, J. H.; Kim, S. H.; Shiratori, S. Fabrication of nanoporous and hetero structure thin film via a layer-by-layer self assembly method for a gas sensor. *Sens. Actuators, B* **2004**, *102*, 241–247.

(10) Hammond, P. T. Engineering materials layer-by-layer: Challenges and opportunities in multilayer assembly. *AIChE J.* **2011**, *57*, 2928–2940.

(11) Su, P.-G.; Lee, C. T.; Chou, C. Y.; Cheng, K. H.; Chuang, Y. S. Fabrication of flexible NO_2 sensors by layer-by-layer self-assembly of multi-walled carbon nanotubes and their gas sensing properties. *Sens. Actuators, B* **2009**, *139*, 488–493.

(12) Xie, G.; Sun, P.; Yan, X.; Du, X.; Jiang, Y. Fabrication of Methane gas sensor by layer-by-layer self-assembly of polyaniline/PdO ultra thin films on quartz crystal microbalance. *Sens. Actuators, B* **2010**, *145*, 373–377.

(13) Su, P. G.; Shiu, C. C. Flexible H_2 Sensor fabricated by layer-by-layer self-assembly of thin films of polypyrrole and modified in situ with Pt nanoparticles. *Sens. Actuators, B* **2011**, *157*, 275–281.

(14) Su, P. G.; Li, W. C.; Tseng, J. Y.; Ho, C. J. Fully transparent and flexible humidity sensors fabricated by layer-by-layer self-assembly of thin film of poly(2-acrylamido-2-methylpropane sulfonate) and its salt complex. *Sens. Actuators, B* **2011**, *153*, 29–36.

(15) Noire, M. H.; Dureault, B. A ferrous ion optical sensor based on fluorescence quenching. *Sens. Actuators, B* **1995**, *29*, 386–391.

(16) Saari, L. A.; Seitz, W. R. Immobilized calcein for metal ion preconcentration. *Anal. Chem.* **1984**, *56*, 810–813.

(17) Thomas, F.; Serratrice, G.; Beguin, C.; Aman, E. S.; Pierre, J. L.; Fontecave, M.; Laulhere, J. P. Calcein as a fluorescent probe for ferric iron. *J. Bio. Chem.* **1999**, *274*, 13375–13383.

(18) Sadaoka, Y.; Sakai, Y.; Murata, Y. Optical humidity and ammonia gas sensor using calcein-based films. *Sens. Actuators, B* **1993**, *13*, 420–423.

(19) Sadaoka, Y.; Sakai, Y.; Wang, X. M. Optical properties of fluorescent dye-doped-polymer thin film and its application to an optochemical sensor for quantification of atmospheric humidity. *J. Mater. Sci.* **1994**, *29*, 883–886.

(20) Kruglenko, I.; Shirshov, Y.; Burlachenko, J.; Savchenko, A.; Kravchenko, S.; Manera, M. G.; Rella, R. Sensitive coating for water vapors detection based on thermally sputtered calcein thin films. *Talanta* **2010**, *82*, 1392–1396.

(21) Li, L.; Ma, R. Z.; Ebina, Y.; Iyi, N.; Sasaki, T. Positively charged nanosheets derived via total delamination of layered double hydroxides. *Chem. Mater.* **2005**, *17*, 4386–4391.

(22) Williams, G. R.; O'Hare, D. Towards understanding, control and application of layered double hydroxide chemistry. *J. Mater. Chem.* **2006**, *16*, 3065–3074.

(23) Evans, D. G., Duan, X., Eds.; *Layered Double Hydroxide (Structure and Bonding)*; Springer-Verlag: Berlin, 2006; p 119.

(24) Xu, Z. P.; Stevenson, G. S.; Lu, C. Q.; Lu, G. Q.; Bartlett, P. F.; Gray, P. P. Stable suspension of layered double hydroxide nanoparticles in aqueous solution. *J. Am. Chem. Soc.* **2006**, *128*, 36–37.

(25) Guo, Y.; Zhang, H.; Wang, Y.; Liao, Z. L.; Li, G. D.; Chen, J. S. Controlled growth and photocatalytic properties of CdS nanocrystals implanted in layered metal hydroxide matrixes. *J. Phys. Chem. B* **2005**, *109*, 21602–21607.

(26) Xu, X.; Lu, R.; Zhao, X.; Xu, S.; Lei, X.; Zhang, F.; Evans, D. G. Fabrication and photocatalytic performance of a $Zn_xCd_{1-x}S$ solid solution prepared by sulfuration of a single layered double hydroxide precursor. *Appl. Catal B-Environ* **2011**, *102*, 147–156.

(27) Fang, X. S.; Bando, Y.; Liao, M. Y.; Zhai, T. Y.; Gautam, U. K.; Li, L.; Koide, Y.; Golberg, D. An efficient way to assemble ZnS nanobelts as ultraviolet-light sensors with enhanced photocurrent and stability. *Adv. Funct. Mater.* **2010**, *20*, 500–508.

(28) Aryal, B. P.; Benson, D. E. Electron donor solvent effects provide biosensing with quantum dots. *J. Am. Chem. Soc.* **2006**, *128*, 15986–15987.

(29) Uezar, N.; Okur, S.; Arikan, M. C. Investigation of humidity sensing properties of ZnS nanowires synthesized by vapor liquid solid (VLS) technique. *Sens. Actuator A* **2011**, *167*, 188–193.

(30) Liu, Y. G.; Feng, P.; Xue, X. Y.; Shi, S. L.; Fu, X. Q.; Wang, C.; Wang, Y. G.; Wang, T. H. Room-temperature oxygen sensitivity of ZnS nanobelts. *Appl. Phys. Lett.* **2007**, *90*, 042109 (3 pages)..
(31) Hasania, M.; Coto Garcia, A. M.; Costa-Fernandez, J. M.; Sanz-Medel, A. Sol−gels doped with polymer-coated ZnS/CdSe quantum dots for the detection of organic vapors. *Sens. Actuators, B* **2010**, *144*, 198−202.
(32) Xu, L.; Song, H.; Zhang, T.; Fan, H.; Fan, L.; Wang, Y.; Dong, B.; Bai, X. A novel ethanol gas sensor-ZnS/cyclohexylamine hybrid Nanowires. *J. Nanosci. Nanotechnol.* **2011**, *11*, 2121−2125.
(33) Adachi-Pagano, M.; Forano, C.; Besse, J. P. Delamination of layered double hydroxides by use of surfactants. *Chem. Commun.* **2000**, 91−92.
(34) Hibino, T.; Jones, W. New approach to the delamination of layered double hydroxides. *J. Mater. Chem.* **2001**, *11*, 1321−1323.
(35) O'Leary, S.; O'Hare, D.; Seeley, G. Delamination of layered double hydroxides in polar monomers: New LDH-acrylate nanocomposites. *Chem. Commun.* **2002**, 1506−1507.
(36) Antonyraj, C. A.; Koilraj, P.; Kannan, S. Synthesis of delaminated LDH: A facile two step approach. *Chem. Commun.* **2010**, *46*, 1902−1904.
(37) Liu, Z. P.; Ma, R. Z.; Osada, M.; Iyi, N.; Ebina, Y.; Takada, K.; Sasaki, T. Synthesis, anion exchange, and delamination of Co−Al layered double hydroxide: Assembly of the exfoliated nanosheet/polyanion composite films and magneto-optical studies. *J. Am. Chem. Soc.* **2006**, *128*, 4872−4880.
(38) Yan, D.; Lu, J.; Wei, M.; Han, J.; Ma, J.; Li, F.; Evans, D. G.; Duan, X. Ordered poly(p-phenylene)/layered double hydroxide ultrathin films with blue luminescence by layer-by-layer assembly. *Angew. Chem., Int. Ed.* **2009**, *48*, 3073−3076.
(39) Yan, D. P.; Lu, J.; Ma, J.; Wei, M.; Evans, D. G.; Duan, X. Reversibly thermochromic, fluorescent ultrathin films with a supramolecular architecture. *Angew. Chem., Int. Ed.* **2011**, *50*, 720−723.
(40) Mu, J.; Zhang, Y. ZnS thin film prepared through a self-assembled thin film precursor route. *Appl. Surf. Sci.* **2006**, *252*, 7826−7829.
(41) Chen, Z.; Cao, M.; Hu, C. Novel Zn_2SnO_4 hierarchical nanostructures and their gas sensing properties toward ethanol. *J. Phys. Chem. C* **2011**, *115*, 5522−5529.
(42) Fan, L. B.; Song, H. W.; Zhao, H. F.; et al. Solvothermal synthesis and photoluminescent properties of ZnS/cyclohexylamine: Inorganic−organic hybrid semiconductor nanowires. *J. Phys. Chem. B* **2006**, *110*, 12948−12953.